Mott polarimetry at JLab: working notes on theory

X. Roca-Maza*
Dipartimento di Fisica, Università degli Studi di Milano and INFN, Sezione di Milano, 20133 Milano, Italy
(Dated: September 23, 2015)

These working notes contain the basic theory employed to obtain the theoretical results used in the calibration of the Mott polarimeter at the Jefferson Laboratory, USA. The presented calculations and notes are based on Refs. [1–4].

I. INTRODUCTION

Elastic collisions of electron projectiles with atoms and ions are usually described by means of the static-field approximation. The target atom is considered as a frozen distribution of charge and the interaction with the projectile is assumed to reduce to the instantaneous Coulomb interaction [5]. Exchange effects, accounting for the occurrence of a rearrangement collision in which the projectile electron exchange place with an atomic electron, can be approximately accounted for by adding an approximate local-exchange interaction [6] to the electrostatic potential. The accuracy of the static-field approximation is limited by inelastic absorption and charge-polarization effects. The existence of open inelastic channels implies a loss of projectile flux from the elastic channel, i.e. a depletion of the elastically scattered wave function. This causes a reduction of the elastic differential cross section (DCS) at intermediate and large angles that can be described approximately by means of an absorptive (negative imaginary) potential. On the other hand, under the action of the electric field of the projectile, the target-charge distribution is polarized, and the electric field of the induced dipole acts back on the projectile. The polarization interaction can be described approximately by means of a local correlation-polarization potential that decreases as r^{-4} at large distances. This interaction affects the elastic DCS mostly at small angles because of the long range of the dipole field. Thus, the effective interaction takes the form of an optical-model potential that consists of the electrostatic interaction, the absorptive imaginary potential and the correlation-polarization potential[1].

Within the static-field approximation, the interaction potential is completely determined by the adopted nuclear and electronic charge-density models. The nuclear charge density of the target nucleus can be modelized by a parametrized function [7] fitted to experiment or derived from microscopic models such as those based on effective interactions solved within the mean-field approach [2, 3]. The latter framework has been shown to be reasonable in the description of bulk nuclear properties along the whole nuclear chart [8]. For incident electron energies of some MeV, parametrized densities that reproduce the experimental charge radius of the studied nucleus or accurate microscopic models predict negligible differences on the scattering observables. Regarding the electronic charge-density in neutral atoms, they are generated using the multiconfiguration Dirac-Fock code of Desclaux [9]. Those correspond to the most accurate electron densities available for free atoms.

A theoretical description of high-precision measurements on electron scattering observables, may require to also account for the so called radiative corrections or quantum electrodynamic (QED) corrections. The lowest order correction in the fine-structure constant consist on the self-energy and the vacuum polarization corrections. For heavy nuclei with a large charge number Z the QED effects cannot be treated perturbatively. Such calculations were performed for the QED corrections to electronic energy levels [10], radiative electron capture in ion-atom collisions [11] or radiative recombination in electron-atom collisions [12]. The self-energy and vacuum-polarization contributions, being of the same order in the expansion on the fine-structure constant, are expected to be of the same order of magnitude. Moreover, they are of opposite sign when evaluated on atomic electrons [12] and, therefore, they are also believed to be of opposite sign in the case of incident electrons. Self-energy corrections are very complicated to be reliably evaluated with high accuracy. They introduce a non-locality in the interaction potential, requires renormalization –divergent terms appear– and, within our approximation, require to work with electron wave functions that are eigenstates of the Coulomb potential and not simple plane waves. On the other side, the vacuum-polarization correction can be more easily estimated by means of the Uehling approximation [13].

The calculations presented here have been performed by using the code ELSEPA [1] and later modifications [2]. The last modification, not published before, corresponds to the inclusion of the Uehling potential to evaluate the effect of the vacuum-polarization correction. ELSEPA allows relativistic partial-wave calculations to be performed for projectiles with kinetic energies up to several MeV and for a variety of interaction potentials. Elastic DCSs and spin-polarization functions calculated in this way constitute the state-of-the-art for energies at the MeV level. For higher energies, the convergence of the partial-wave series becomes too slow and the code has recourse to approximate factorization methods that

* xavier.roca.maza@mi.infn.it
[1] For electron energies of the order of few MeV the absorptive and correlation-polarization effects become negligible.

permit the calculation of electron DCSs up to few GeV.

These notes are organized as follows. In Sec.II, a review of the theory necessary to produce the results shown in Sec.III is briefly discussed. Our conclusions are laid in Sec.IV.

II. THEORY

We consider here the elastic interaction of an electron with a target atom—or ion—of atomic number Z placed at the origin of coordinates. We have assumed that the charge distribution of the target is spherically symmetric. The effective interaction between the electron at a distance r and the target is described by means of an optical-model potential,

$$V(r) = V_{\rm st}(r) + V_{\rm ex}(r) \ , \tag{1}$$

where $V_{\rm st}(r)$ is the electrostatic interaction potential and $V_{\rm ex}(r)$ is an exchange potential that accounts for the occurrence of rearrangement collisions in which the projectile electron exchange place with an atomic electron [6]. We do not take into account here the correlation-polarization potential which is only needed for slow projectiles, with E less than about 10 keV. We do not consider an imaginary absorption potential to modelize the loss of particles from the elastic channel to inelastic channels since it may affect the scattering amplitudes for beam energies up to about 1 MeV, depending on the target atomic number [1]. In addition, owing to the assumed spherical symmetry of the atomic charge distribution, the potential and all its components are also spherical. Then, elastic-scattering properties can be calculated by using conventional partial-wave methods [1].

The potential energy of an electron at a distance r from the center of the nucleus is given by

$$\begin{aligned} V_{\rm st}(r) &\equiv -e\varphi(r) \equiv -e[\varphi_{\rm nucl.}(r) + \varphi_{\rm at.elec.}(r)] \qquad (2)\\ &= -4\pi e \left(\frac{1}{r}\int_0^r \rho_{\rm n}(r')\, r'^2 {\rm d}r' \, + \int_r^\infty \rho_{\rm n}(r')\, r' {\rm d}r' \right) \\ &\quad -4\pi e \left(\frac{1}{r}\int_0^r \rho_{\rm e}(r')\, r'^2 {\rm d}r' \, + \int_r^\infty \rho_{\rm e}(r')\, r' {\rm d}r' \right) \end{aligned}$$

where $\rho_{\rm n}(r)$ denotes the charge density of the nucleus normalized to Z and $\rho_e(r)$ that of atomic electrons normalized to Z for neutral atoms—and to the total number of electrons for ions. At the energies of interest, the effect of screening by the orbiting atomic electrons is limited to small scattering angles.

To quantify the screening of the nuclear charge by the atomic electrons, it is customary to introduce the screening function, $\chi(r)$, defined as the fraction of the nuclear charge seen by a particle at a distance r from the center of the nucleus,

$$\chi(r) \equiv \frac{r}{Ze}\varphi(r) \tag{3}$$

Evidently, for neutral atoms the screening function vanishes for large r. For a positive ion with N orbiting electrons ($N < Z$), the screening function at large distances tends to the constant value $1 - N/Z$, i.e. far from the ion the potential is Coulombian. The electrostatic potential and the particle densities of the atom are linked by Poissons equation which for spherically symmetric systems and $r > 0$ simplifies to

$$\rho_{\rm n}(r) - \rho_{\rm e}(r) = -\frac{Z}{4\pi r}\frac{{\rm d}^2\chi(r)}{{\rm d}r^2} \tag{4}$$

In the cases in which the effects of the atomic electrons can be neglected, since the nuclear charge density is assumed to vanish beyond a certain radius $r_{\rm B}$ (i.e. the radius of the box where the nuclear charge distribution is calculated), the potential (3) is purely Coulombian, $V(r) = -Ze^2/r$, beyond that radius. Globally it can be regarded as a Coulomb potential with the short-range distortion arising from the finite size of the nucleus, i.e., as a modified Coulomb potential.

The DCS for elastic scattering of spin unpolarized electrons is given by

$$\frac{{\rm d}\sigma}{{\rm d}\Omega} = |f(\theta)|^2 + |g(\theta)|^2, \tag{5}$$

where

$$\begin{aligned} f(\theta) = \frac{1}{2{\rm i}k}\sum_{\ell=0}^{\infty} \Big\{ & (\ell+1)\left[\exp\left(2{\rm i}\delta_{\kappa=-\ell-1}\right) - 1\right] \\ & + \ell\left[\exp\left(2{\rm i}\delta_{\kappa=\ell}\right) - 1\right] \Big\} P_\ell(\cos\theta) \end{aligned} \tag{6}$$

and

$$\begin{aligned} g(\theta) = \frac{1}{2{\rm i}k}\sum_{\ell=0}^{\infty} \Big[& \exp\left(2{\rm i}\delta_{\kappa=\ell}\right) \\ & - \exp\left(2{\rm i}\delta_{\kappa=-\ell-1}\right) \Big] P_\ell^1(\cos\theta) \end{aligned} \tag{7}$$

are the direct and spin-flip scattering amplitudes, respectively. Here k denotes the wave number of the projectile electron,

$$c\hbar k = \sqrt{E(E + 2m_{\rm e}c^2)}, \tag{8}$$

and the functions $P_\ell(\cos\theta)$ and $P_\ell^1(\cos\theta)$ are Legendre polynomials and associated Legendre functions, respectively. The phase shifts δ_κ represent the behavior of the Dirac spherical waves at large r distances. Relative numerical uncertainties of the computed scattering amplitudes and DCS are estimated from the convergence of the partial-wave series, they are typically smaller than 10^{-6}. ELSEPA also provides the Sherman function—or analyzing power,

$$S(\theta) \equiv \imath\frac{f(\theta)g^*(\theta) - f^*(\theta)g(\theta)}{|f(\theta)|^2 + |g(\theta)|^2} \tag{9}$$

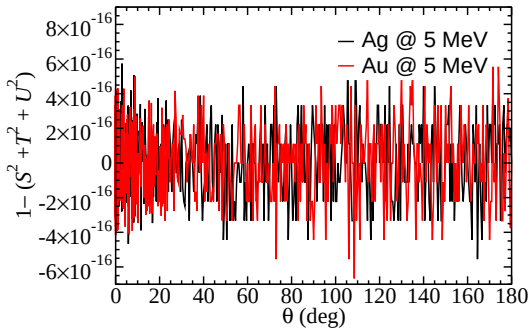

FIG. 1. Sum rule as a function of the scattering angle for two test cases: 5 MeV electron beam on a Ag and Au targets.

which gives the degree of spin polarization of the electrons from an initially unpolarized beam that are scattered in the direction θ.

Also important are the spin rotation functions $T(\theta)$ and $U(\theta)$,

$$T(\theta) \equiv \frac{|f(\theta)|^2 - |g(\theta)|^2}{|f(\theta)|^2 + |g(\theta)|^2} \tag{10}$$

$$U(\theta) \equiv \frac{f(\theta)g^*(\theta) + f^*(\theta)g(\theta)}{|f(\theta)|^2 + |g(\theta)|^2} \ . \tag{11}$$

The square of the spin functions should fulfill the sum rule $S(\theta)^2 + T(\theta)^2 + U(\theta)^2 = 1$. This sum rule may be also used as an alternative test to the numerical accuracy of the employed method. For the calculations shown in Sec.III, the sum rule departs from 1 within a 10^{-15} relative error (cf. Fig.1 were we show two test cases).

For modified Coulomb potentials, the spherical solutions of the Dirac equation are suitably expressed in the form

$$\psi_{E\kappa m}(\mathbf{r}) = \frac{1}{r}\begin{pmatrix} P_{E\kappa}(r)\,\Omega_{\kappa,m}(\hat{\mathbf{r}}) \\ \mathrm{i}Q_{E\kappa}(r)\,\Omega_{-\kappa,m}(\hat{\mathbf{r}}) \end{pmatrix}. \tag{12}$$

The functions $\Omega_{\kappa,m}(\hat{\mathbf{r}})$ are the spherical spinors, and the radial functions $P_{E\kappa}(r)$ and $Q_{E\kappa}(r)$ satisfy the following system of coupled differential equations:

$$\frac{\mathrm{d}P_{E\kappa}}{\mathrm{d}r} = -\frac{\kappa}{r}P_{E\kappa} + \frac{E - V + 2m_\mathrm{e}c^2}{c\hbar}\,Q_{E\kappa},$$

$$\frac{\mathrm{d}Q_{E\kappa}}{\mathrm{d}r} = -\frac{E - V}{c\hbar}\,P_{E\kappa} + \frac{\kappa}{r}Q_{E\kappa}. \tag{13}$$

The relativistic quantum number κ is defined as $\kappa = (\ell - j)(2j + 1)$, where j and ℓ are the total and orbital angular momentum quantum numbers. Note that j and ℓ are both determined by the value of κ; $j = |\kappa| - 1/2$, $\ell = j + \kappa/(2|\kappa|)$. In the numerical calculations, the spherical waves are normalized so that the upper-component radial function $P_{E\kappa}(r)$ oscillates asymptotically with unit amplitude.

For modified Coulomb potentials and $r \to \infty$, we have (see, e.g., Ref. [1] and references therein)

$$P_{E\kappa}(r) \simeq \sin\left(kr - \ell\frac{\pi}{2} - \eta\ln 2kr + \delta_\kappa\right), \tag{14}$$

where

$$\eta = Ze^2m_\mathrm{e}/(\hbar^2 k) \tag{15}$$

is the Sommerfeld parameter. It is convenient to express the phase shifts δ_κ as $\Delta_\kappa + \hat{\delta}_\kappa$, where Δ_κ is the phase shift of the point-nucleus Coulomb potential and $\hat{\delta}_\kappa$ is the "inner" phase shift of the short-range potential induced by the nuclear charge distribution.

As indicated above, the calculations reported here have been performed using the computer code ELSEPA [1]. It solves the radial Dirac equations using a robust integration algorithm which effectively minimizes the effect of truncation errors. The algorithm starts from a table of values of the function $rV(r)$ at the points r_i of a radial grid, which is provided by the user. This function is replaced by the natural cubic spline that interpolates the tabulated values; thus, in the interval between consecutive grid points, the potential function $rV(r)$ is represented as a cubic polynomial. The radial wave equations (13) are then solved by using the exact power-series expansions of the radial functions. The integration is started at $r = 0$ and extended outwards up to a point r_m that is beyond the starting radius r_B of the Coulomb tail. The phase shift $\hat{\delta}_\kappa$ is determined by matching the outer analytical form to the inner numerical solution at r_m, requiring continuity of the radial function $P_{E\kappa}(r)$ and its derivative. The regular and irregular Dirac-Coulomb functions and their derivatives are accurate to more than 10 decimal figures.

The convergence rate of the series (6) and (7) for the calculation of $\mathrm{d}\sigma/\mathrm{d}\Omega$ is known to be slow. The summations are optimized by performing them in two steps [1]. First, they are evaluated for the pure Coulomb field, for which the phase shifts Δ_κ are known analytically and the calculation is fast. Second, the point-nucleus results are subtracted from the expansions (6) and (7); the remaining series represent the effect of only the short-range component of the potential and converge more rapidly than the original series. As a consequence, the number of inner phase shifts $\hat{\delta}_\kappa$ one needs to compute is normally much smaller than the number of required Coulomb phase shifts.

A. The nuclear charge distribution

The details of the nuclear charge distribution affect the calculated scattering observables only for projectiles with kinetic energies larger than about 50 MeV for which the de Broglie wavelength is comparable to the nuclear radius. For lower energies, it is a good approximation to consider the nuclear distribution using simplified models such as the two parameter Fermi function or the Helm model [2, 3]. Of course, for very low impact energies, the nucleus can be considered as point-like.

We have modelized the nuclear charge density by

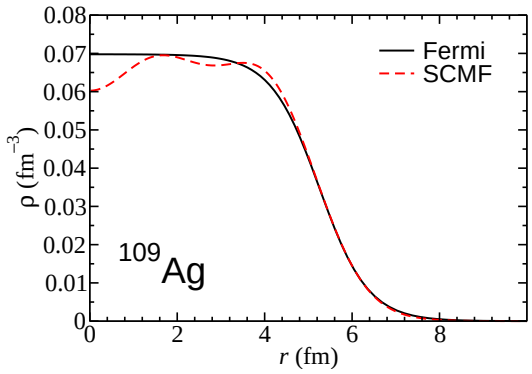

FIG. 2. Nuclear charge density as a function of the distance to the center for Ag. A Fermi model and a self-consistent mean-field model are shown.

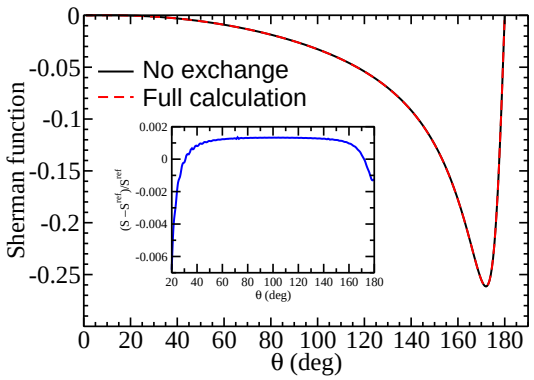

FIG. 3. Sherman function of 5 MeV electrons on a Ag target as a function of the scattering angle. Calculations represented by the solid black line neglect the effect of the exchange potential while the ones represented by a dashed red line include such an effect. In the inset, the relative difference is depicted.

means of a two parameter Fermi function,

$$\rho_{\rm F}(r) = \frac{\rho_0}{1+\exp[(r-C)/a]} \tag{16}$$

where ρ_0 is determined by fixing the charge of the nucleus (Z); a describes the diffuseness of the surface of the density profile; and C describes the mean location of this surface (i.e., C is indicative of the extension of the bulk part of the density distribution). We have determined a and C so that they reproduce the experimental root mean square charge radius, $\langle r^2_{\rm ch}\rangle^{1/2}$ of 4.5601 ± 0.0035 fm and 5.4371 ± 0.0038 fm, for ^{109}Ag and ^{197}Au, respectively [14]. Specifically, the parameters of the Fermi function are $a = 0.5573$ fm and $C = 5.250$ fm for Ag and $a = 0.58187$ fm and $C = 6.440$ fm for Au. As an example, in Fig.2 we show the charge density corresponding to ^{109}Ag. For comparison we show also the prediction of a self-consistent mean-field model (SCMF [15]).

The Fermi distribution has a very simple functional form, which is enough for the study of few MeV incident electrons. It displays the correct surface fall-off behavior when compared to experiment and more sophisticated calculations such as (SCMF). On this regard, we have checked that an accurate nuclear self-consistent mean-field model give the same result within 0.1 % error in the Sherman function (cf. inset of Fig.7) when compared with the fitted Fermi and Helm distributions at the kinematics and target nuclei we are interested in.

As a final remark, the mean-field approach is accurate for the description of bulk properties of nuclei. It assumes that nucleons move independently in a mean field generated by the other nucleons of the atomic nucleus. Different effective interactions solved at the mean-field exist [8]. These phenomenological models usually depend on about ten adjustable parameters that are fitted to reproduce relevant ground-state properties, such as binding energies and charge radii of a few nuclei. For recent works that analyze the accuracy of mean field models in the description of the DCS in elastic electron scattering, we refer the reader to Ref.[2].

B. Electron density model

We have adopted the most accurate electron densities available for free atoms obtained from self-consistent relativistic Dirac-Fock (DF) calculations [9]. The effect in the Sherman function of neglecting atomic electrons in scattering processes of few MeV electrons may produce an error of about a few % (cf. Fig.7).

C. Electron exchange potentials

When the projectile is an electron, we must account for the occurrence of rearrangement collisions in which the projectile exchanges places with an atomic electron. In an elaborate formulation of relativistic-electron elastic scattering, the system of the projectile and the atomic electrons is described by a wave function with the form of a single Slater determinant. Then, the scattering wave function is found to satisfy an equation similar to the Dirac-Fock equations, with a non-local exchange term that is difficult to handle. A simpler, and computationally more convenient approach (static-exchange approximation) is to use local approximations to the exchange interaction. Specifically, we have used the Furness-McCarthy exchange potential [16]. It is derived directly from the formal expression of the non-local exchange interaction by using a WKB-like approximation for the wave functions. The effect in the Sherman function of neglecting the effect of the exchange potential in scattering processes of few MeV electrons may produce an error of about a few ‰ (cf. Fig.3). So negligible for our purposes.

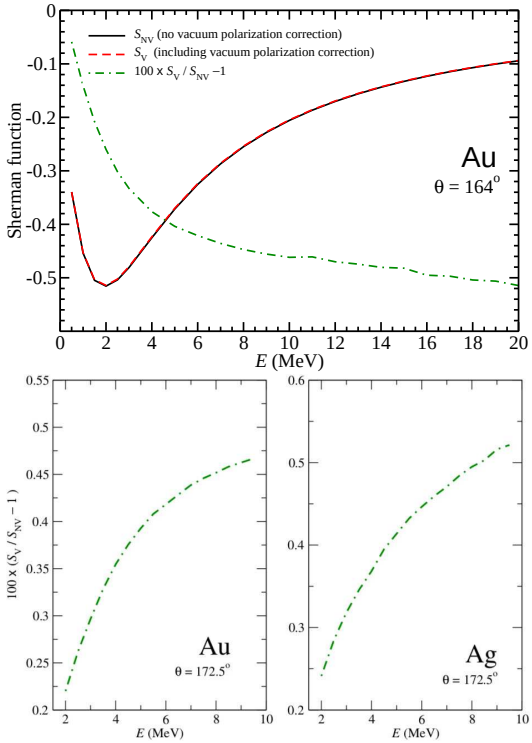

FIG. 4. Sherman function dependence on electron beam energy at forward angles and the relative difference when compared to the effect of the vacuum polarization corrections to the same quantity.

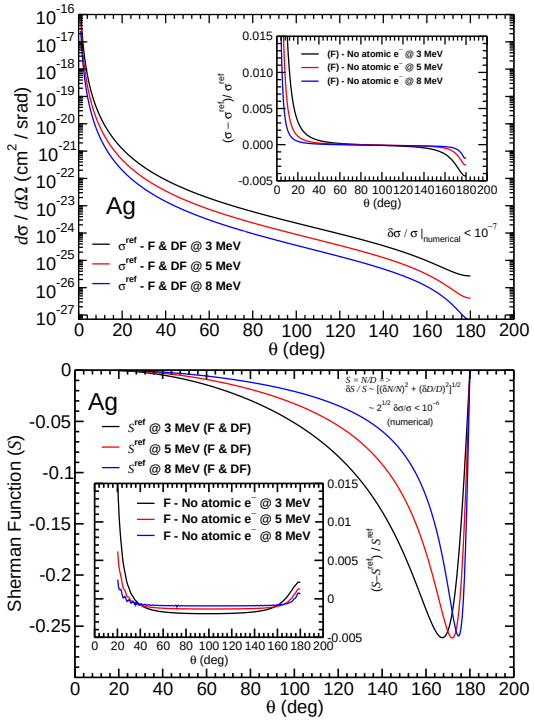

FIG. 5. Elastic differential cross section (upper panel) and Sherman function (lower panel) as a function of the scattering angle for 3, 5 and 8 MeV electrons by Ag. In the insets, the relative change of the same quantity when the energy increases are displayed.

D. QED corrections

We evaluate the vacuum polarization correction by following the Uehling approximation [13] but, instead of doing it perturbatively, the Dirac equation is solved in the combined potential[2]. That is, we add the potential due to the vacuum-polarization effects to $V(r)$. Specifically, the vacuum polarization correction is of 0.5% or below (increases with energy) for the kinematics and target in which we are interested in (cf. Fig.4). As previously mentioned, the leading QED corrections (of order fine structure constant times Z) consist of the self-energy and the vacuum polarization corrections. Since both corrections are of the same order and of different sign [12], then, one may estimate the correction to the Sherman function due to the leading QED corrections. So, we do not include in our calculation the vacuum polarization correction but use it in order to estimate the accuracy of our theoretical predictions.

We note that it might be misleading to include such a correction in the calculations and neglect the self-energy correction: both are leading QED corrections—of the same order in the fine structure constant—and both should be included for a fully consistent calculation.

[2] We follow exactly the strategy explained in Ref.[4]

E. Final remarks

Breemsstrahlung and recoil effects might be a relevant issue on these scattering processes. Nevertheless, we have neglected such effects in the calculations. One of the reasons is that these effects can be corrected in the simulations of the experimental data by using GEANT4 (is this correct?). The same applies for other issues such as the real thickness of the target.

On the other side, we have checked with different codes the numerical accuracy and method discrepancies in our results finding that it is within the 0.1% accuracy. Taking into account all the previous considerations, the theoretical results used for calibration of the Mott polarimeter are accurate within (about) a 0.5% in the region of interest. We note that the main theoretical error is coming from the effect of QED corrections.

III. RESULTS

In this section we present some of the results obtained for the DCS and Sherman function in elastic scattering of few MeV electrons by Ag and Au. First of all we show some test of the calculations described in Sec.II. In Fig.5 the elastic DCS (upper panel) and the Sherman function (lower panel) as a function of the scattering an-

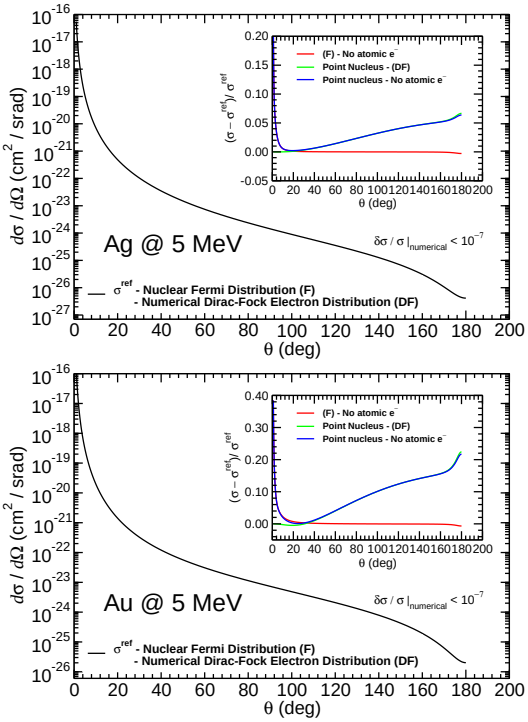

FIG. 6. Elastic differential cross section as a function of the scattering angle for 5 MeV electrons by Ag (upper panel) and Au (lower panel). In the inset, the relative change of the same quantity adopting different approximations and with respect the full calculation is displayed.

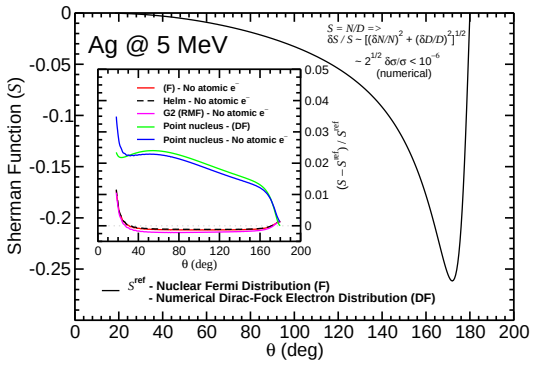

FIG. 7. Sherman function dependence on the scattering angle for 5 MeV electrons by Au. In the inset, the relative change of the same quantity adopting different approximations and with respect the full calculation is displayed.

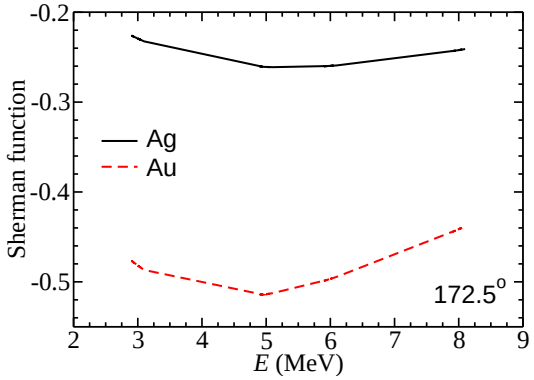

FIG. 8. Sherman function dependence on the electron beam energy for Ag and Au at 172.5 deg.

gle for 3, 5 and 8 MeV electrons by Ag are shown. The results correspond to calculations where all ingredients have been included—except for the vacuum polarization corrections; F means that the Fermi function is used to modelized the nuclear charge distribution; and DF stands for the model used for taking into account the effects the atomic electrons. The DCS decreases with energy. In the insets, we show the relative change of the same quantities with respect to the case in which the presence of atomic electrons is neglected. The insets highlight, thus, the effect of atomic electrons on the DCS and Sherman function, which is negligible except for small angles.

In Fig.6 we display the elastic differential cross section as a function of the scattering angle for 5 MeV electrons and Ag (upper panel) and Au (lower panel) targets. The results correspond to calculations where all ingredients explained in Sec.II have been included. In the inset, the relative change of the same quantity adopting different approximations and with respect the full calculation is displayed: neglecting atomic electrons (red); assuming a point-like nucleus (blue); and adopting the last two approximations (green). It is clear from the inset, that neglecting the finite size of the nucleus may produce a large error of few tens of % in the DCS. It is also evident that the effect of atomic electrons is much less relevant.

In Fig.7 we show the Sherman function dependence on the scattering angle for 5 MeV electrons and Ag (upper panel) and Au (lower panel) targets. In the inset, the relative change of the same quantity adopting different approximations and with respect the full calculation are displayed: assuming a point-like nucleus with (green) and without (blue) accounting for the presence of atomic electrons; and neglecting atomic electrons and assuming different models describing the finite size of the nuclear charge distribution: Fermi model (red), Helm model (black) and SCMF (magenta) named G2. Similar results to those obtained for the DCS are also found here. While the effect of accounting or note for the presence of atomic electrons is almost irrelevant for our purposes, the finite size of the nucleus may produce a change on the Sherman function of few %.

In Fig.8, we show the dependence of the Sherman function on the electron beam energy around 5 MeV and for a scattering angle of 172.5 deg for Ag and Au targets.

IV. CONCLUSIONS

We believe the calculations are realistic within (about) a 0.5% in the Sherman function for the kinematics and

targets of interest. The main source of theoretical uncertainties comes from the leading QED corrections or radiative corrections which have been roughly estimated to produce about a 0.5% discrepancy in the Sherman function.

ACKNOWLEDGMENTS

We would like to kindly thank D. H. Jakubassa-Amundsen for useful discussions and numerical tests.

[1] F. Salvat, A. Jablonski, and C. J. Powell, Computer Physics Communications **165**, 157 (2005).
[2] X. Roca-Maza, M. Centelles, F. Salvat, and X. Viñas, Phys. Rev. C **78**, 044332 (2008).
[3] X. Roca-Maza, M. Centelles, F. Salvat, and X. Viñas, Phys. Rev. C **87**, 014304 (2013).
[4] D. Jakubassa-Amundsen, "The influence of vacuum polarization on the sherman function during elastic electron-nucleus scattering," (2014), arXiv:1407.6809.
[5] H. S. W. Massey and N. F. Mott, "Theory of atomic collisions," (Oxford University Press, 1965).
[6] B. H. Bransden, M. R. C. McDowell, C. J. Noble, and T. Scott, Journal of Physics B: Atomic and Molecular Physics **9**, 1301 (1976).
[7] R. W. Hasse and W. D. Myers, "Geometrical relationships of macroscopic nuclear physics," (Springer-Verlag, Heidelberg, 1988).
[8] M. Bender, P.-H. Heenen, and P.-G. Reinhard, Rev. Mod. Phys. **75**, 121 (2003).
[9] J. Desclaux, Computer Physics Communications **9**, 31 (1975).
[10] G. Soff and P. J. Mohr, Phys. Rev. A **38**, 5066 (1988).
[11] T. Beier, A. N. Artemyev, J. Eichler, V. M. Shabaev, and V. A. Yerokhin, Physica Scripta **1999**, 322 (1999).
[12] V. M. Shabaev, V. A. Yerokhin, T. Beier, and J. Eichler, Phys. Rev. A **61**, 052112 (2000).
[13] E. A. Uehling, Phys. Rev. **48**, 55 (1935); L. W. Fullerton and G. A. Rinker, Phys. Rev. A **13**, 1283 (1976).
[14] I. Angeli, Atomic Data and Nuclear Data Tables **87**, 185 (2004).
[15] G. A. Lalazissis, T. Nikšić, D. Vretenar, and P. Ring, Phys. Rev. C **71**, 024312 (2005).
[16] J. B. Furness and I. E. McCarthy, Journal of Physics B: Atomic and Molecular Physics **6**, 2280 (1973).